Article

Atlantic overturning inferred from air-sea heat fluxes indicates no decline since the 1960s

Jens Terhaar [1,4,5] ✉, Linus Vogt [1,2] & Nicholas P. Foukal [1,3]

The Atlantic Meridional Overturning Circulation (AMOC) is crucial for global ocean carbon and heat uptake, and controls the climate around the North Atlantic. Despite its importance, quantifying the AMOC's past changes and assessing its vulnerability to climate change remains highly uncertain. Understanding past AMOC changes has relied on proxies, most notably sea surface temperature anomalies over the subpolar North Atlantic. Here, we use 24 Earth System Models from the Coupled Model Intercomparison Project Phase 6 (CMIP6) to demonstrate that these temperature anomalies cannot robustly reconstruct the AMOC. Instead, we find that air-sea heat flux anomalies north of any given latitude in the North Atlantic between 26.5°N and 50°N are tightly linked to the AMOC anomaly at that latitude on decadal and centennial timescales. On these timescales, air-sea heat flux anomalies are strongly linked to AMOC-driven northward heat flux anomalies through the conservation of energy. On annual timescales, however, air-sea heat flux anomalies are mostly altered by atmospheric variability and less by AMOC anomalies. Based on the here identified relationship and observation-based estimates of the past air-sea heat flux in the North Atlantic from reanalysis products, the decadal averaged AMOC at 26.5°N has not weakened from 1963 to 2017 although substantial variability exists at all latitudes.

The Atlantic Meridional Overturning Circulation (AMOC) is an essential part of the global ocean overturning circulation[1] and determines large-scale weather and climate around the North Atlantic[2–11]. The northward limb of the AMOC transports warm and saline water to the high-latitude North Atlantic where this water cools, densifies, and sinks to form the deep southward limb of the AMOC. The AMOC accounts for around 20–30% of the global meridional heat transport (MHT) from the Tropics to high latitudes in the atmosphere and ocean[12]. By transporting large amounts of heat northward, the AMOC exhibits a strong control on the climate in North America and Europe, such as the relatively mild European temperatures and large-scale precipitation

patterns[13,14]. Moreover, the North Atlantic deep-water formation caused by the cooling of the northward-flowing saline waters[15–17] plays a crucial part in the global climate and the carbon cycle by transporting carbon and heat from the atmosphere and surface ocean into the deep ocean[13,18–23]. The sensitivity of North Atlantic deep-water formation to the northward transport of salinity also makes the AMOC a potential tipping element in the climate system and its tipping would have substantial effects on the global and regional climate[24,25].

The importance of the AMOC has motivated multiple reconstructions of AMOC variability via direct observations[1,26–28], proxies[29–35], and models[11,36–38]. Direct observations of the AMOC have

[1]Woods Hole Oceanographic Institution, Woods Hole, MA, USA. [2]Laboratoire d'Océanographie et du Climat Expérimentations et Approches Numériques (LOCEAN), Sorbonne Université, CNRS/IRD/MNHN, Paris, France. [3]Skidaway Institute of Oceanography, University of Georgia, Savannah, GA, USA. [4]Present address: Climate and Environmental Physics, Physics Institute, University of Bern, Bern, Switzerland. [5]Present address: Oeschger Center for Climate Change Research, University of Bern, Bern, Switzerland. ✉e-mail: jterhaar@whoi.edu

been taken, for example, at the RAPID array at 26.5°N since 2004[1,26] and at the Overturning in the Subpolar North Atlantic Program (OSNAP) array around 55°N since 2014[28]. These direct observations present a reference for proxy and model studies and have already demonstrated the large seasonal, inter-annual, and decadal variability of the AMOC[19,27,39–41]. However, these observational records are not long enough to differentiate between low-frequency variability and long-term trends[39,42], which is crucial to detect potential human influence on the large-scale ocean circulation over the industrial period.

A differentiation between low-frequency variability and long-term trends may be achieved by proxies, which provide a longer-term perspective on past AMOC variability and trends. Among the proxies that have been used to reconstruct the strength of the AMOC over the last decades and centuries are surface ocean density anomalies[35], isotopes in foraminifera[31] and corals[33], salinity in the South Atlantic[43], and sea surface temperature (SST) anomalies in the subpolar gyre relative to northern hemispheric or global SSTs[32,34]. This last proxy identifies the observed cooling or lack of warming in the subpolar SST compared to global SSTs over the past century – the "warming hole" - as evidence of a reduced northward MHT caused by a reduced AMOC[32,34]. The relationship between the AMOC anomalies and subpolar gyre SST anomalies with respect to global SSTs (here called the SPG SST index) was calibrated by Caesar et al. with climate models from phase 5 of the Coupled Model Intercomparison Project (CMIP5) and then exploited with observed SPG SST anomalies since 1870[34]. Based on this reconstruction, the AMOC at 26.5°N was estimated to have declined over the last 70 years with a trend of −1.7 Sverdrup (Sv, 10^6 m^3 s^{-1}) per century[34]. Declines of the AMOC of weaker or even stronger magnitude have also been estimated based on a variety of other proxies[29,44].

This concept of exploiting a relationship between an observable and a non-observable variable - in this case, AMOC strength and SPG SST anomalies - with observations has been widely applied in climate science under the name of emergent constraints[22,45–49]. Emergent constraints reduce uncertainties of projections[48–51] and estimate past and present variables or processes that cannot be directly observed[22,34,48]. In the emergent constraint approach, models are not used to determine the unknown variable but to determine the slope and intercept of a relationship between two variables. Thus, each model has equal weight in determining that relationship even if a model does not correctly reproduce the historical trajectory of each variable. In fact, the larger the spread in the variables across the models, the more robustly one can estimate the underlying relationship that is postulated to link the two variables. In the past, however, a number of such relationships that were identified across CMIP5 model ensembles have been later discarded as they were not reproducible across CMIP6 model ensembles[49,52]. These relationships were not reproducible because either the mechanism underlying the assumption was incorrect and the statistical relationship occurred by chance[52] or newly included processes in CMIP6 models, which had not been not adequately been included in CMIP5 models, have altered or broken the assumed relationship[49,52]. Given the large amount of data and models across CMIP ensembles, relationships can emerge by chance[53–55]. Consequently, it has been postulated that a relationship can only be exploited with observations if that relationship is mechanistically plausible, if the underlying mechanism is verifiable, and if the relationship is replicable in any other model ensemble[56,57].

Despite the emergent constraint reconstruction of Caesar et al.[34] suggesting a decreasing AMOC over the last 70 years, recent studies argue that the AMOC has not yet significantly declined over the last centuries and decades[35,39,40,58–60] and that the SPG SST is not a good indicator of AMOC variability[61–63]. Reconstructions of the AMOC based on temperature and salinity observations, for example, demonstrate large decadal and inter-annual variability of the AMOC but no significant reduction over time[35,58,59]. Furthermore, it has been shown that SPG SST anomalies can also be driven by air-sea heat flux anomalies

from the atmosphere and heat transport anomalies towards the Arctic Ocean without associated changes in the AMOC so that the SPG SST anomalies might be a weak proxy for the AMOC strength[64]. In addition, large decadal variabilities in the AMOC and SPG SST at present are likely still too large for a weakening trend to emerge[39,40].

Here, we build on the concept of the SPG SST as an AMOC index[32,34] by extending the concept to account for heat released from the ocean to the atmosphere. Instead of using SST anomalies in a pre-defined region, we construct a heat budget to identify a relationship between the AMOC anomaly at a given latitude and the air-sea heat flux anomaly north of that latitude in the North Atlantic basin across an ensemble of 24 climate models from CMIP6 (Supplementary Table 1). We then exploit this relationship with observation-based estimates from reanalysis products ERA5[65] and JRA-55[66] to reconstruct the decadal averaged AMOC anomaly since 1963.

Results
The subpolar gyre sea surface temperature index in CMIP6
When calculating the SPG SST index with CMIP6 models in the same way as it was done for CMIP5 models[34], a relationship between trends in the SPG SST index from 1870 to 2016 and trends of the AMOC from 1870 to 2016 emerges (Fig. 1) as previously shown[67]. While the existence of this relationship corroborates the underlying link between the AMOC and the SPG SST index, the coefficient of determination (r^2) of the relationship of 0.5 is substantially smaller than the one that was found for the CMIP5 ensemble (0.90)[34]. However, the high coefficient of determination across the 12 models from CMIP5 might have been a consequence of the relatively small number of simulations that were used to calibrate the relationship between the SPG SST index and the AMOC[34]. When including 4–5 times more CMIP5 model simulations[67], a
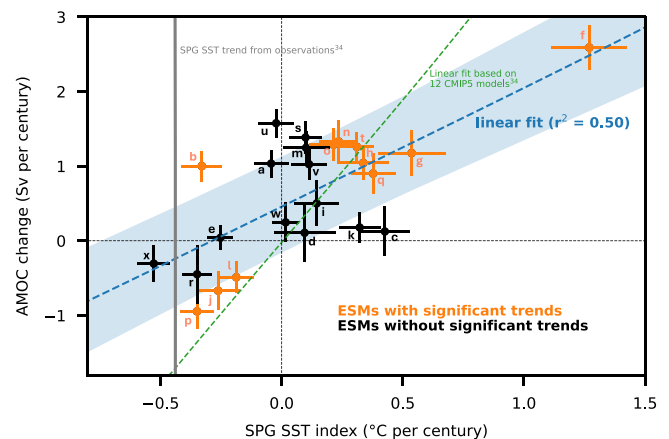

Fig. 1 | Relationship between trends in the AMOC at 26.5°N and the SPG SST index from 1870 to 2016 across 24 climate models from CMIP6. Trends of the Atlantic Meridional Overturning Circulation (AMOC) at 26.5°N and subpolar gyre sea surface temperature (SPG SST) index as calculated by Caesar et al.[34] from 1870 to 2016 (circles) with the uncertainties (1-σ) of the trends (lines). Climate models where trends in both the AMOC and SPG SST index are statistically significant ($p < 0.05$) are shown in orange and climate models where the trends in the AMOC and/or the SPG SST index are not statistically significant are shown in black. The labels at the dots allow identifying the individual earth system models (ESMs): a) CanESM5-CanOE, b) CanESM5, c) CMCC-CM2-SR5, d) CMCC-ESM2, e) CNRM-CM6-1-HR, f) CNRM-CM6-1, g) CNRM-ESM2-1, h) ACCESS-ESM1-5, i) ACCSS_ACCESS-CM2, j) MPI-ESM1-2-HR, k) IPSL-CM6A-LR, l) MIROC6, m) HadGEM3-GC31-LL, n) HadGEM3-GC31-MM, o) UKESM1-0-LL, p) MPI-ESM1-2-LR, q) MRI-ESM2-0, r) GISS_GISS-E2-1-G, s) CESM2, t) CESM2-WACCM, u) NorESM2-LM, v) NorESM2-MM, w) GFDL-CM4, x) GFDL-ESM4. A linear fit (dashed blue line) was calculated across all climate models with the associated projection uncertainty (1-σ) (blue shading). The observed trend of the SPG SST index as calculated by Caesar et al.[34] is shown as a grey line. The linear fit across 12 climate models from CMIP5[34] is shown as a green dashed line.

similar spread as across the CMIP6 ensemble appears. It thus appears that the AMOC affects the SPG SST index as postulated[32,34], but that the link is indeed weaker than expected.

The weaker than previously assumed relationship is likely due to mechanisms that affect either the AMOC or the SPG SST index but not both at the same time[61–63] and due to the different locations of the warming hole. In the CMIP6 ensemble, 10 of the 24 climate models have a statistically significant ($p < 0.05$) trend in one variable and no statistically significant trend in the other (Fig. 1, Supplementary Figs. 1 and 2). Some models show, for example, a change in the SPG SST index without an associated change in the AMOC, which might be a consequence of a potentially overly strong sensitivity to aerosol forcing in some CMIP6 models[67]. Although the aerosol sensitivity might be too strong in the CMIP6 models, the resulting SPG SST change should also result in an associated AMOC change if both variables were strongly linked. While aerosols are one example of how the AMOC and the SPG SST index can be affected independently, there are likely others[61–63], such as air-sea heat flux anomalies from the atmosphere and heat transport anomalies towards the Arctic Ocean[64]. Another reason for these weak correlations might be that the pre-defined SPG region covers an area that is substantially larger than the 'warming holes' or 'warming hotspots' in most climate models (Supplementary Fig. 3). Thus, SST noise in the large remaining part of the SPG may obscure the actual signal.

Not only is the relationship across the 24 CMIP6 models substantially weaker than previously estimated based on 12 CMIP5 model simulations[34], but the slope and intercept of the relationship also vary between both model ensembles. In the CMIP5 ensemble[34], the slope of the relationship (3.8 Sv K^{-1}) is more than twice as large as it is in the CMIP6 ensemble (1.6 Sv K^{-1}), and the intercept (0.0 Sv) is smaller in the CMIP5 ensemble than in the CMIP6 ensemble (0.5 Sv). The larger intercept might be a consequence of the relatively large impact of aerosols on the AMOC and the relatively small or even opposite impact of aerosols on SPG SSTs[67]. As a consequence of the different slopes and intercepts, the observed change in the SPG SST index from 1870 to 2016 of −0.44 °C per century results in a trend of the AMOC of −0.2 ± 0.7 Sv per century when using the CMIP6 models, which is not significantly different from zero, and substantially smaller than the trend of −1.7 Sv per century found for CMIP5[34] and not significantly different from zero. The results based on the CMIP5 model ensemble cannot thus be reproduced with the CMIP6 model ensemble, indicating that the relationship is too uncertain to enable robust reconstructions of AMOC trends over the last century and beyond.

Even if the AMOC and SPG SST trends are weak on centennial timescales, strong variability in the AMOC might permit tighter constraints on the relationship between the AMOC and SPG SST index, and allow SST-based reconstructions of the past AMOC on annual or decadal timescales[39]. However, the relationship between the AMOC and the SPG SST index across the CMIP6 model ensemble is also small to almost non-existent on annual ($r^2 = 0.15$), decadal ($r^2 = 0.30$), and centennial ($r^2 = 0.12$) timescales over the historical period (Fig. 2a), indicating that the SPG SST index is not a robust proxy for AMOC variability for the past. Nevertheless, a relationship between the AMOC and the SPG SST index emerges over the 21st century when anomalies of the AMOC and the SPG SST index are large (Fig. 2b, c). This emerging relationship demonstrates that the underlying mechanism between AMOC, MHT, and SPG SST anomalies exists. However, for a robust SST anomaly to emerge within the SPG across climate models from CMIP6, the AMOC decline must be substantial (>±1.5 Sv, for example, CNRM-CM6-1 in Fig. 1). Consequently, a reconstruction of the decadal averaged AMOC based on the AMOC-SPG SST index relationship results in uncertainties of more than ±2 Sv and similarly large deviations between the directly simulated and reconstructed AMOC (Supplementary Fig. 4). Overall, it seems to be impossible to identify AMOC anomalies in the range of ±1.5 Sv based on the SPG SST index and

climate models from CMIP6, and even more so to derive potential tipping of the AMOC based on variability in the SPG SST index[68,69].

North Atlantic Ocean heat budget

While the relationship between anomalies of the AMOC and the SPG SST index on annual, decadal, or centennial timescales appears weak, a strong relationship exists between AMOC anomalies at a given latitude and air-sea heat flux anomalies in the North Atlantic north of that latitude on decadal to centennial timescales (Fig. 3). This relationship between AMOC anomalies and air-sea heat flux anomalies is physically linked to the heat budget over the North Atlantic Ocean (Fig. 4) and has been identified in observations[70]. Here we define the North Atlantic as the region bounded by the combination of Davis Strait, Fram Strait, and Barents Sea Opening to the north and bounded in the south by the latitude where the AMOC anomaly is to be determined.

Generally, a regional ocean heat budget can be written as heat content change in that region being equal to the sum of the fluxes across the region's boundary:

$$\frac{dOHC}{dt} = -\nabla \cdot HT + \iint Q_{net} \, d\lambda \, d\theta \qquad (1)$$

where OHC is the Ocean Heat Content integrated vertically over the full ocean depth, and spatially over a region of interest, HT is the horizontal heat transport across the horizontally bounding faces, and Q_{net} is the surface heat flux (W m^{-2}) with λ and θ representing the longitude and latitude. When the region of interest is bounded zonally by land and marginal seas, as is true for the large-scale North Atlantic heat budget, the divergence of HT is simplified to the meridional heat transport (MHT) across the southern face minus the transport across the northern face. Here, we consider the North Atlantic heat budget as:

$$\frac{dOHC}{dt} = MHT_{south} - MHT_{Arctic} + \iint Q_{net} \, d\lambda \, d\theta, \qquad (2)$$

where MHT_{south} refers to the northward MHT over the southern latitude of the region and MHT_{Arctic} refers to the northward MHT into the Arctic. MHT_{Arctic} is calculated here as the residual of the other three components that were available as model output. In this study, we calculate the budget for the North Atlantic north of the latitudes 26.5°N, 30°N, 35°N, 40°N, 45°N, 50°N, and 55°N, and bounded to the north by Davis Strait, Fram Strait, and the Barents Sea Opening. In equilibrium, i.e., without global warming, the long-term averaged $\frac{dOHC}{dt}$ is zero and the three fluxes compensate each other. MHT in the North Atlantic decays strongly northward from a peak of around 1.2 PW at 26.5°N to around 0.5 PW at 50°N[71,72] due to heat loss from the ocean to the atmosphere. The largest anomalies across the components of the North Atlantic heat budget over the historical period are simulated in the southern MHT (1.6 ZJ yr^{-1}, mean of absolute values between 1850 and 2014) and surface heat flux (1.4 ZJ yr^{-1}) terms, while anomalies in heat storage (0.7 ZJ yr^{-1}) and Arctic MHT (0.4 ZJ yr^{-1}) are smaller (Fig. 5). The southern MHT and surface heat fluxes are the dominant heat budget components in all models, although individual models simulate different magnitudes and frequencies of the variability. These differences might be explained by a different base state of the North Atlantic across models, as the projected decline in the AMOC is also state-dependent[36,73], or by different internal variability, for example, internal changes in ocean circulation[74], or sensitivities to external drivers, such as atmospheric driven air-sea heat fluxes, across the model ensemble[75–77]. Independent of the driver and magnitude of the variability of the components of the North Atlantic heat budget, a change in the southern MHT over the historical period is largely compensated in climate models by a change in surface heat fluxes and
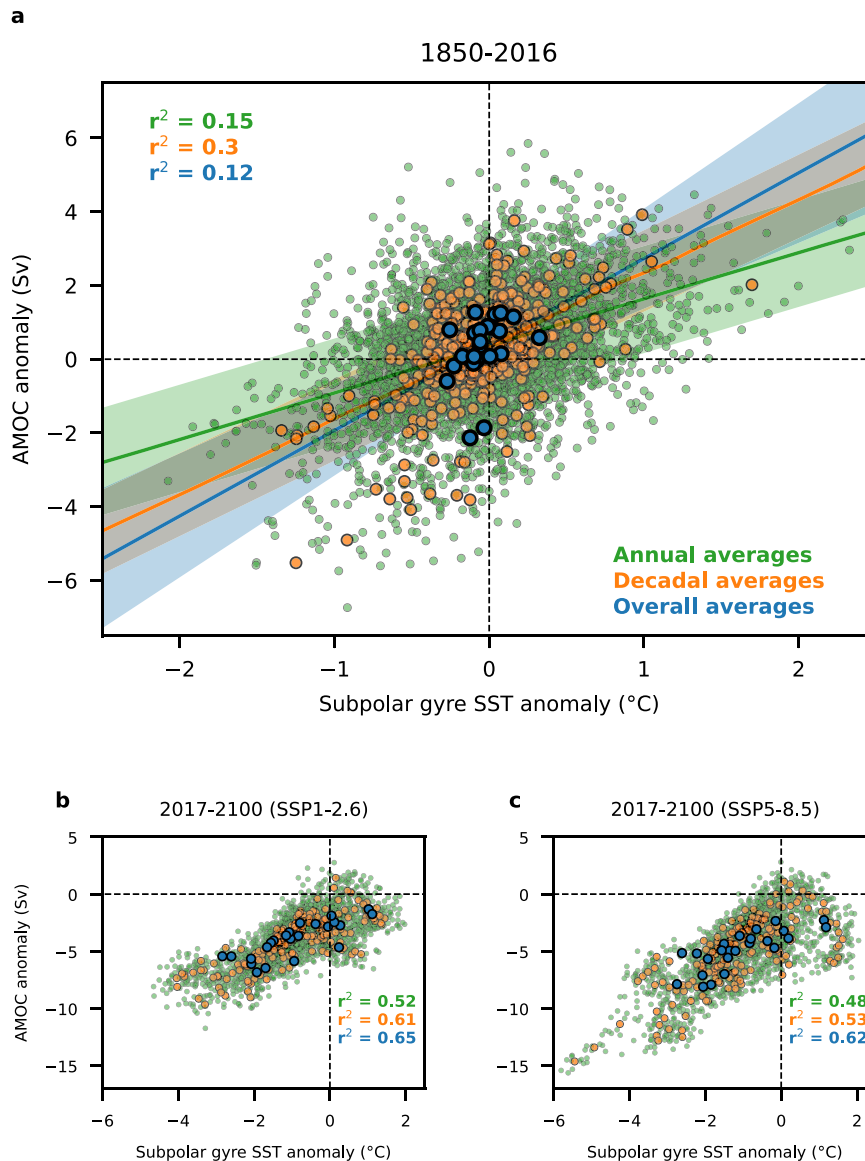
Fig. 2 | AMOC anomalies at 26.5°N vs Atlantic subpolar gyre SST anomalies across climate models from CMIP6 at various timescales. The Atlantic Meridional Overturning Circulation (AMOC) anomalies are calculated at 26.5°N for 24 climate models individually with respect to a linear trend over the time period in the pre-industrial AMOC simulations of each model that corresponds to the time period in the historical simulations. The subpolar gyre sea surface temperature (SPG SST) anomalies following Caesar et al. [34] are calculated with respect to a linear trend over the time period in the pre-industrial AMOC simulations of each model that corresponds to the time period in the historical simulations. Blue dots indicate averages of the respective anomalies from **a** 1850 to 2016, and from 2017 to 2100 under **b** SSP1-2.6 and **c** SSP5-8.5. Orange dots indicate decadal averages of the anomalies from **a** the 1850s to the 2010s, and from **b, c** the 2020s to the 2090s. Green dots show annual averaged anomalies from **a** 1850 to 2016, and **b, c** from 2017 to 2100. Only the relationship for overall averages in (**a**) is not statistically significant.

less so by a change in the ocean heat content or the heat flux toward the Arctic Ocean[78].

The dominance of these two anomalies in the North Atlantic heat budget and the strong relationship between the AMOC and southern MHT lead to the tight relationship between AMOC anomalies and air-sea heat flux anomalies even for AMOC changes smaller than ±1.5 Sv (Fig. 3). Across the ensemble of 18 climate models from CMIP6, the AMOC variability at 26.5°N is strongly related to the annual ($r^2 = 0.84$), decadal ($r^2 = 0.94$), and centennial ($r^2 = 0.98$) variability of northward MHT at the same latitude (Fig. 6b). The relationship between the AMOC and the southern MHT is strong because the variability of the volume of the water transported northward by the AMOC is much larger than the variability of the temperature of that water[79–81]. The variability of southern MHT anomaly is then linked to the variability of the air-sea heat flux in the North Atlantic on decadal ($r^2 = 0.71$) and

centennial timescales ($r^2 = 0.93$) (Fig. 6a). On annual timescales, however, the southern MHT anomaly is only very weakly linked to the variability of the air-sea heat flux in the North Atlantic ($r^2 = 0.19$). This weak link on annual timescales suggests that other terms such as the change in OHC could be important, and atmospheric dynamics override the overall importance of southern MHT from the tropical Atlantic Ocean[70,82,83]. However, on longer timescales, the oceanic variability dominates so that the southern MHT anomalies are strongly linked to air-sea heat flux anomalies. As a result, the North Atlantic air-sea heat flux anomalies are a close proxy for AMOC anomalies on decadal and centennial timescales (Figs. 3 and 5).

The heat budget method is distinct from the frequently used Walin framework[84–86], which infers ocean circulation from surface buoyancy fluxes. The Walin framework aggregates the water mass transformation between sets of outcropping isopycnals and
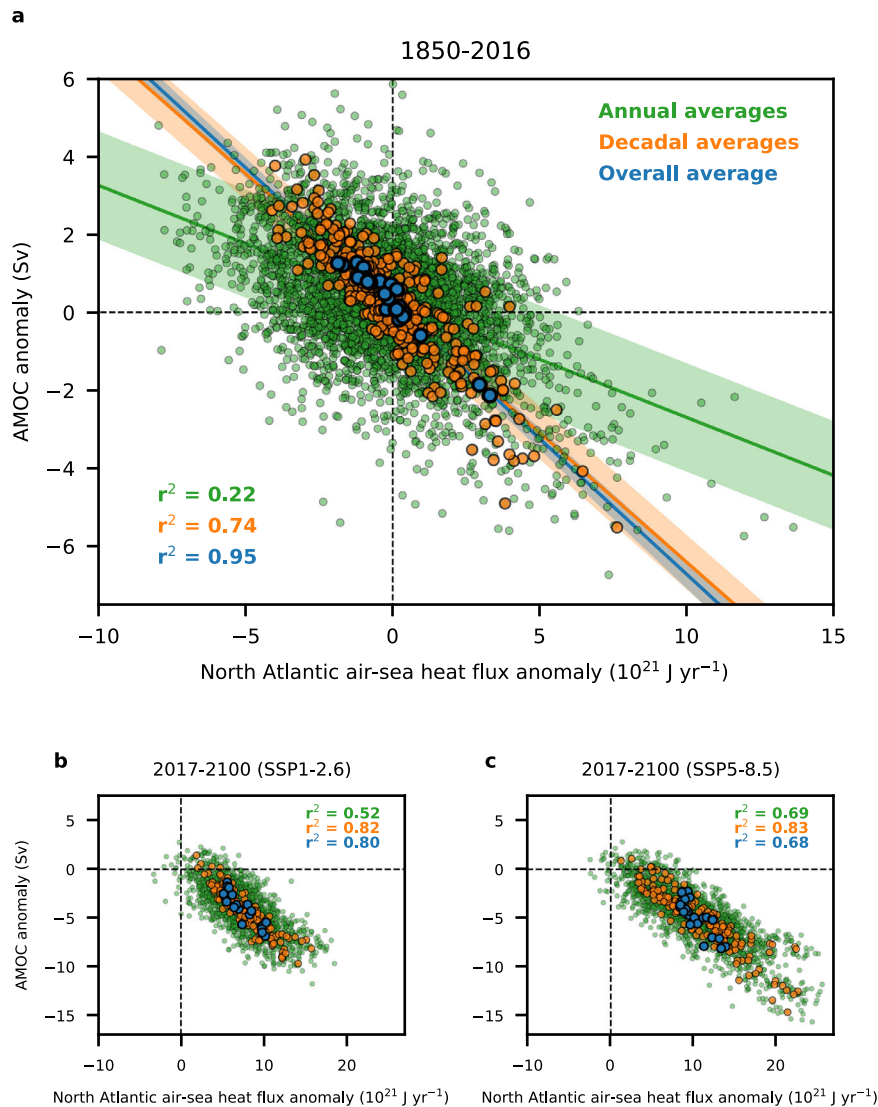
Fig. 3 | AMOC anomalies at 26.5°N vs air-sea heat flux anomalies north of 26.5°N across climate models from CMIP6 at various timescales. The Atlantic Meridional Overturning Circulation (AMOC) anomalies are calculated at 26.5°N for 24 climate models individually with respect to a linear trend over the time period in the pre-industrial AMOC simulations of each model that corresponds to the time period in the historical simulations. The North Atlantic air-sea flux anomalies north of 26.5°N and south of the Arctic (see orange area in Fig. 4 and methods for a detailed definition of the region) are calculated with respect to linear trend over the time period in the pre-industrial AMOC simulations of each model that corresponds to the time period in the historical simulations. Blue dots indicate averages of the respective anomalies from **a** 1850 to 2016, and from 2017 to 2100 under **b** SSP1-2.6 and **c** SSP5-8.5. Orange dots indicate decadal averages of the anomalies from **a** the 1850s to the 2010s, and from **b**, **c** the 2020s to the 2090s. Green dots show annual averaged anomalies from **a** 1850 to 2016, and **b**, **c** from 2017 to 2100. Positive heat flux anomalies indicate an increased heat flux from the atmosphere into the ocean.

implies a causal relationship in which the surface buoyancy fluxes force the ocean dynamics[86–91]. As opposed to the Walin framework, the heat budget mechanism described here relies on surface heat fluxes and does not provide information about a causal relationship; these fluxes are simply connected through Eq. (2). Although a lead-lag correlation analysis of the climate models from CMIP6 shows that air-sea heat fluxes lead the AMOC on average by around 3 years (Supplementary Fig. 5), similar correlations exist also for a lead of air-sea heat fluxes by 10 years and for a lead by the AMOC by 7 years. As different mechanisms appear to be linking the AMOC and air-sea heat flux anomalies[86–93], we do not attempt to infer a causal relationship and simply rely on the heat budget that averages over these lead/lag relationships and holds on decadal timescales. A second advantage of the heat budget approach is that it is a bulk estimate integrated over a wide geographic region and thus avoids the same spatial biases as the SPG SST index (Supplementary Fig. 3).

Spatially, the maximum coefficient of determination (r^2) between the AMOC and the heat flux anomalies occurs in the subpolar North Atlantic, similar to the maximum r^2 between the AMOC and SST anomalies (Fig. 7). The similarity between the spatial patterns underlines that changes in air-sea heat fluxes and SPG SST are linked. However, the local r^2 is higher when using heat fluxes instead of SST (compare panels a and b in Fig. 7), suggesting that air-sea heat fluxes dampen the SST changes and are thus more tightly connected to the AMOC. Previous studies have also found that changes in the MHT in the western part of the subpolar gyre are strongly compensated by air-sea heat fluxes[78,94].

Testing the capability of air-sea heat fluxes to reconstruct the AMOC using climate models

To test how well air-sea heat fluxes can reconstruct decadal AMOC anomalies simulated by each model, we calculated a linear regression and 1-σ prediction intervals over decadal averaged anomalies of the
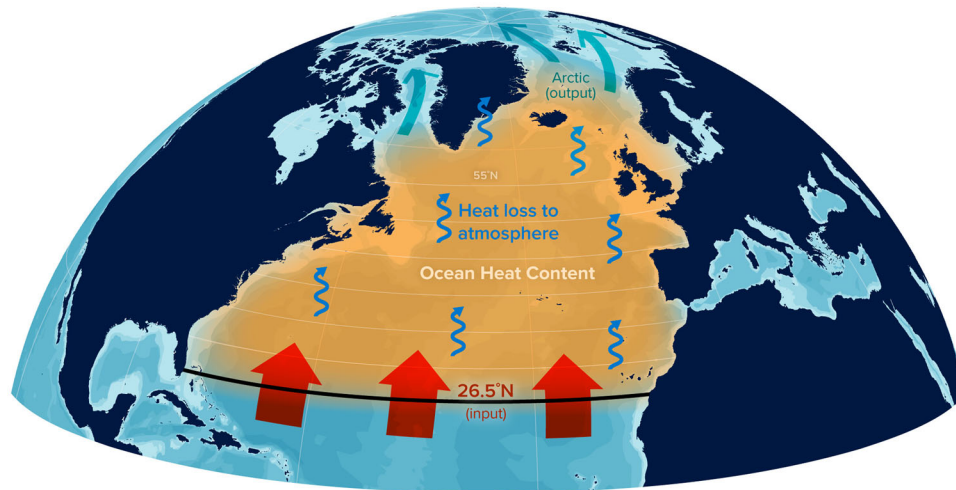
Fig. 4 | Schematic representation of the North Atlantic heat budget. Heat transport into the region from the south (red) can be compensated by: (1) heat transport out of the region to the north (green), (2) heat loss to the atmosphere (blue), or (3) a change in Ocean Heat Content (orange).

AMOC and of the air-sea heat flux (as shown in Fig. 3) across all climate models but one. We then combined this relationship with the directly simulated air-sea heat flux anomaly from the climate model that was excluded from the fit to estimate that model's AMOC anomalies (Fig. 8, Supplementary Fig. 6). The comparison between the reconstructed and directly simulated AMOC demonstrates that the air-sea heat flux anomalies can indeed be used to reconstruct the net AMOC anomalies until the 1990s and that the reconstruction provides an upper limit that diverges at most 1 Sv from the net AMOC anomaly afterwards. The heat fluxes detect (1) long-term decadal AMOC variabilities as in CMCC-CM2-SR5 (Fig. 8c), (2) AMOC increases around 2000 as in HadGEM3-GC31-LL (Fig. 8m), and (3) AMOC reductions in recent decades as in GFDL-CM4 (Fig. 8w). While the reconstruction is not perfect, e.g., the variability of the reconstructed AMOC can be too low (e.g., Fig. 8l, r) or too high (Fig. 8s, t), the directly simulated AMOC is within the 2-sigma range of the reconstructed AMOC for 95% of all years, which is expected for a normally distributed error term. Also, the horizontal model resolution does not appear to change the ability to reconstruct the AMOC, as differences between the directly simulated and the reconstructed AMOC are not substantially different between models of different resolutions (see for example the GFDL, MPI, CNRM, and HadGEM models in Fig. 8 and Supplementary Fig. 6). To further corroborate the relationship between AMOC and air-sea heat flux anomalies, we also successfully tested the relationship using the pre-industrial control simulations (Supplementary Figs. 7 and 8) and climate models from CMIP5 (Supplementary Fig. 9) (see "Methods" section for details). The consistency in the relationship between air-sea heat flux anomalies and AMOC anomalies across CMIP5 and CMIP6 model ensembles despite the difference in the effect of aerosol forcing between CMIP5 and CMIP6 models[67] further supports the finding that air-sea heat fluxes and the AMOC are indeed mechanistically connected.

After 1990–2000, the air-sea heat flux-based reconstructions provided an upper limit as indicated by a too-weak reconstructed AMOC in comparison to the directly simulated AMOC in some historical simulations after 1990–2000, when ocean heat uptake started to accelerate[95]. This additional air-sea heat flux anomaly due to anthropogenic warming incorrectly results in a decline of the reconstructed AMOC in these climate models (Fig. 8), and is hence not visible in the reconstructions across the pre-industrial control simulations (Supplementary Figs. 7 and 8). Such a difference between the directly simulated and the reconstructed AMOC is larger than 1 Sv and exceeds the 2-sigma range in models with high equilibrium climate

sensitivities (ECSs), for example, CanESM5, CanESM5-CanOE, IPSL-CM6A-LR, or UKESM1-0-LL (Fig. 8 and Supplementary Fig. 6)[96]. These models all share an ECS that exceeds the recently assessed likely range[97]. The excessive ECS in these climate models has led to an overly strong warming over the recent decades[96]. This strong atmospheric warming then leads to additional air-sea heat flux into the Atlantic Ocean (Fig. 5 and Supplementary Fig. 10). As the historic warming and the ECSs are outside of observed and assessed ranges[96–98], we interpret this mismatch as an exception, rather than the rule of the surface flux reconstruction method. Hence, we conclude that the identified relationship across climate models between AMOC and air-sea heat flux anomalies can be used with confidence until 1990–2000 but may be biased low by up to 1 Sv over the last 20–30 years.

In the future, stronger atmospheric warming and associated ocean heat uptake (Fig. 3b, c, and Supplementary Fig. 10) will further increase the difference between the simulated and reconstructed AMOC based on air-sea heat flux anomalies. While these reconstructions still provide an upper limit for an AMOC decline, air-sea heat fluxes due to atmospheric warming will need to be considered in the coming decades.

Reconstructing the historical AMOC with observation-based air-sea heat flux anomalies

We now use observation-based estimates of the North Atlantic air-sea heat flux anomaly north of 26.5°N from reanalysis products to reconstruct the historical AMOC variability at 26.5°N. Here, we use annual air-sea heat fluxes in the North Atlantic from ERA5[65] and JRA-55[66] to create a timeseries of the decadal averaged AMOC over the satellite period from 1958 to 2022. Although ERA5 extends until 1940, we here rely only on the period when both reanalysis datasets provide data and comparisons can be made between products.

Based on the observation-based air-sea heat flux estimates, we confirm the absence of an overall trend of the AMOC but find decadal variability. The AMOC reconstructions at 26.5°N using ERA5 and JRA-55 (Fig. 9a) suggest a relatively stable AMOC over the last decades with anomalies fluctuating between ±2 Sv. This variability is much smaller than the AMOC variability in climate models (Fig. 8). Across both reconstructions, a positive trend for the AMOC at 26.5°N can be found from 1963 to 2017 of 0.022 ± 0.005 Sv per decade (ERA5) and 0.022 ± 0.003 Sv per decade (JRA-55). The uncertainties (shading in Fig. 9) are solely based on the linear fit (Fig. 3) and do not include the uncertainties of the observation-based surface heat flux anomalies themselves[99]. Due to the size of these uncertainties, the detected
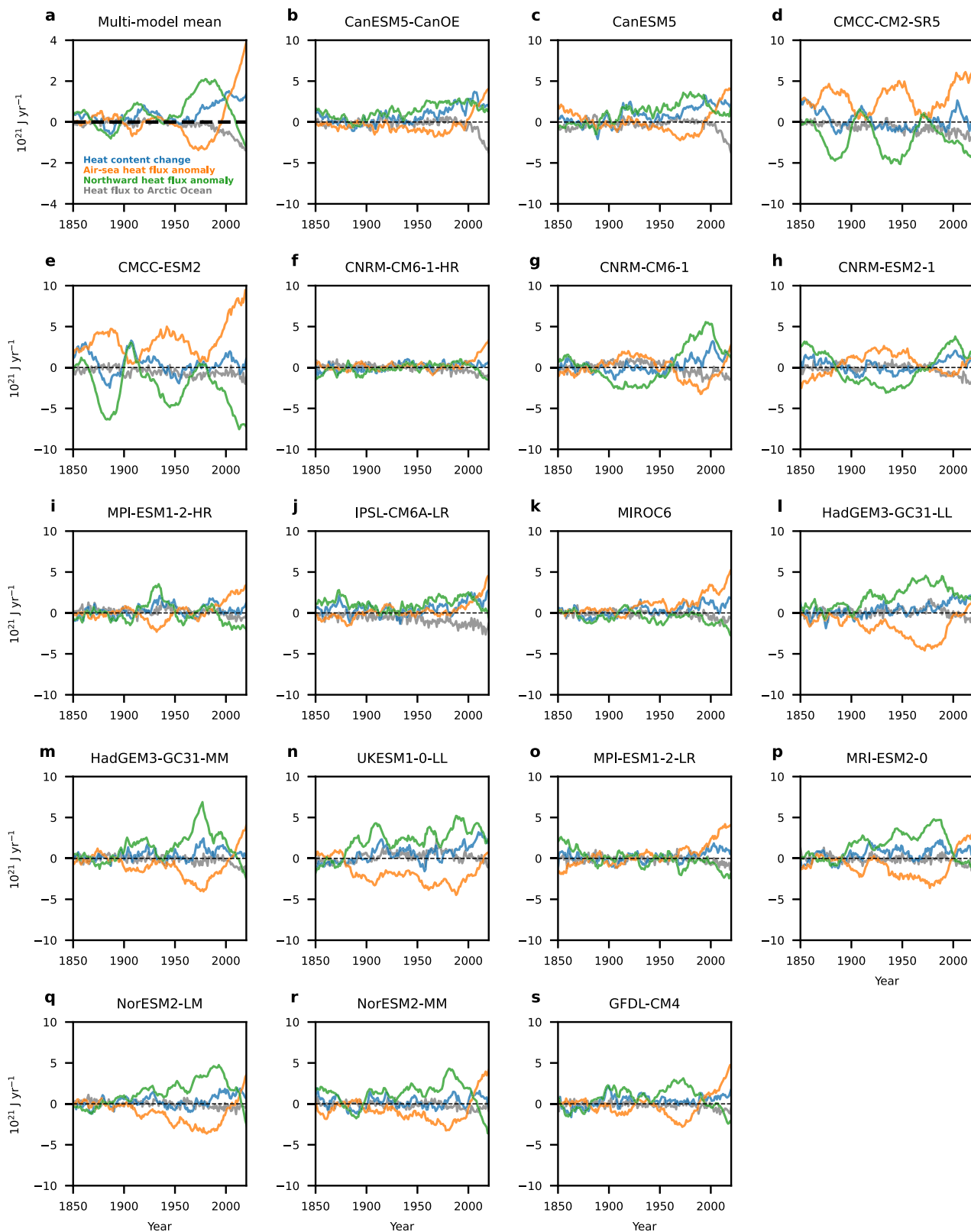
Fig. 5 | Historical decadal variability of the North Atlantic heat budget north of 26.5°N from 1850 to 2020. Timeseries smoothed with a 11-year running mean (±5 years) of the North Atlantic ocean heat content change north of 26.5°N (blue), the anomaly of the air-sea heat flux in the same region (orange), the anomaly of the northward heat flux at 26.5°N (green), and the residual representing the heat flux to the Arctic Ocean (grey) for the **a** multi-model mean across an ensemble of 18 climate models and **b**–**s** for each model individually. The missing 6 climate models from the total ensemble of 24 climate models did not provide the northward heat transport and are therefore not shown here.
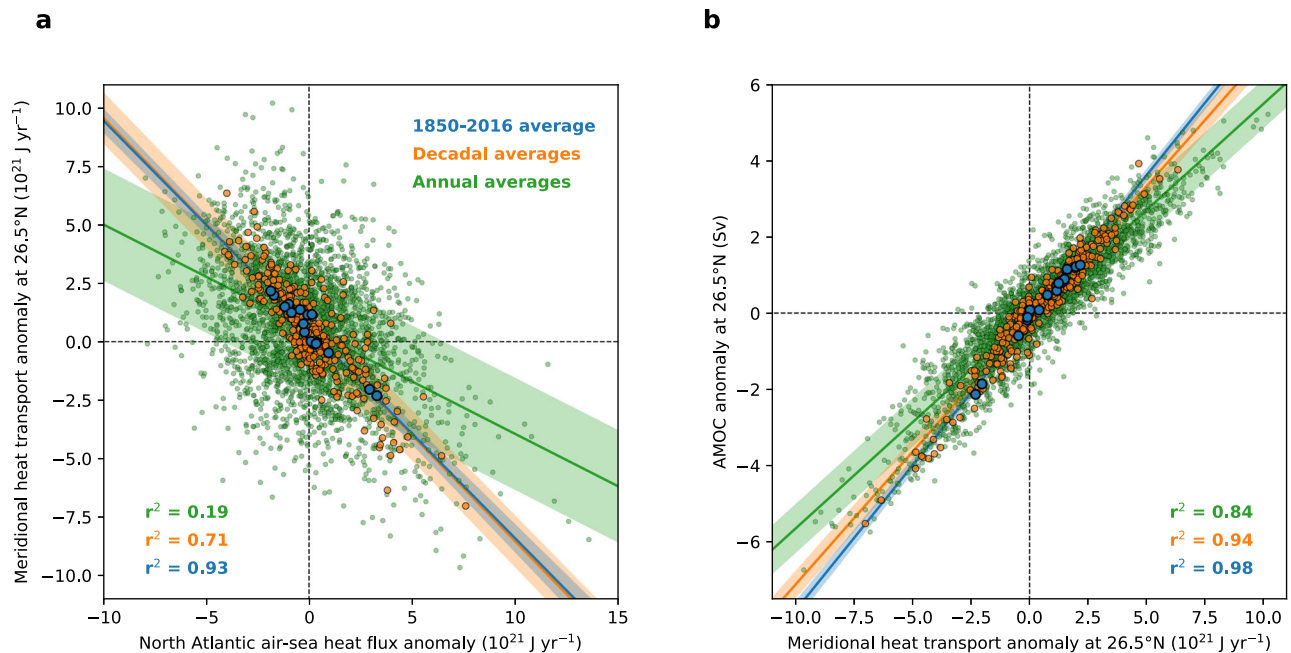
Fig. 6 | Meridional heat transport anomalies across 26.5°N compared to North Atlantic air-sea heat flux north of 26.5°N, and AMOC anomalies at 26.5°N. Correlations are shown **a** between southern meridional heat transport (MHT) anomalies and North Atlantic air-sea heat flux anomalies, and **b** between southern MHT anomalies and Atlantic Meridional Overturning Circulation (AMOC) anomalies. AMOC and northward heat flux anomalies are calculated at 26.5°N for 18 climate models individually with respect to each climate model pre-industrial AMOC.

The North Atlantic air-sea flux anomalies in the north of 26.5°N are calculated with respect to each climate model's pre-industrial air-sea heat fluxes for each model individually. Blue dots indicate averages of the respective anomalies from 1850 to 2016, orange dots indicate decadal averages of the anomalies from the 1850s to the 2010s, and green dots show annual averaged anomalies from 1850 to 2016. A positive heat flux anomaly indicates an increased heat flux from the atmosphere into the ocean.

trends are likely not statistically significant. However, a negative trend is unlikely, especially given that atmospheric warming would lead to a negative bias in the reconstructed AMOC over this period.

The reconstructed AMOC timeseries from ERA5 and JRA-55 both exhibit decadal variability. The timeseries show a slight increase in the AMOC from 1995 to 2005 followed by a slight decrease afterwards (Fig. 9). Before 1995, the AMOC reconstructions diverge, especially over the subtropics (26–35°N), though they remain within the uncertainties. This difference between the reconstructions, which is not statistically significant, could be due to the differences in the representation of aerosols, which strongly influence the atmosphere and heat budget in the North Atlantic. In ERA5, aerosols evolve over time based on an observation-based forcing that was developed for CMIP5[65], whereas aerosols in JRA-55 are prescribed as a constant climatology[66]. Instead, JRA-55 indirectly incorporates variability in aerosols through its data assimilation of observations, which are subject to realistic aerosol forcing.

As we can only reconstruct decadal variability with this method, a comparison to directly observed decadal AMOC variability based on observations from the RAPID array from 2005 to 2022 is only possible for the years 2010–2017. Although this is a very short period and we do not place much emphasis on this relationship, the small decline over this period of the AMOC in observations is in line with the decline over the same period in the ERA5 and JRA-55 reconstructions.

Reconstructing the AMOC anomaly at various latitudes
Reconstructing the AMOC anomalies with air-sea heat fluxes also has the benefit that it allows reconstructing the AMOC at any latitude in the North Atlantic (Fig. 9). Across the ensemble of 24 climate models, we find an r^2 above or equal to 0.7 for decadal averaged values from 26.5°N to 45°N. North of 45°N, the relationships become weaker with r^2 decreasing to 0.63 at 50°N and 0.39 at 55°N (Table 1). At such high latitudes, there are two effects that reduce the correlations: (1) the

MHT through the southern face is less dominant over the MHT into the Arctic so the air-sea heat fluxes are not as strongly related to AMOC anomalies anymore, and (2) the relationship between the AMOC defined in depth coordinates and MHT breaks down[100]. Much of the MHT at these latitudes is carried by the horizontal circulation patterns, and it is more instructive to consider the AMOC in density coordinates[101–104]. Since the density-coordinate AMOC is only provided by a few CMIP models[105], we restrict our analysis to depth coordinates. On longer timescales, the r^2 values over the period from 1850 to 2016 decline from above 0.9 at 45°N to 0.86 at 50°N and 0.66 at 55°N. The still relatively high r^2 for averages over such a long period even at higher latitudes suggest that the MHT to the Arctic Ocean induces additional decadal variability at high latitudes but a weaker long-term signal than AMOC changes.

Overall, the reconstructions of the decadal averaged AMOC anomalies from 30°N to 55°N show different trends and decadal variability from 1963 to 2017. Trends increase from 26.5°N to 40°N, where they reach 0.35 ± 0.03 Sv per decade (ERA5) and 0.46 ± 0.07 Sv per decade (JRA-55). At these latitudes, multidecadal variability is likely strong[58], and thus a longer record would be required to detect a trend. Our AMOC reconstruction at 45°N is similar to that derived from hydrographic data[58] in that it has a weak AMOC centred around 1970 and a strong AMOC in the 1980s and 1990s, weakening in the 2000s. It seems to differ however from the subpolar AMOC reconstructions in Jackson et al. [39] extending back to 1993, and is instead more in line with the AMOC reconstruction at 50°N from forced models[39,106]. This latter result also holds for the subtropical AMOC indices reported in Jackson et al. [107]. Further north, these trends decrease to 0.02 ± 0.01 Sv per decade (ERA5) and 0.17 ± 0.04 Sv per decade (JRA-55). As opposed to the long-term trends, the decadal variability dampens towards higher latitudes. The different time-evolutions at different latitudes highlight that the AMOC is not a simple conveyor belt but more complex and heterogeneous across latitudes[101,108,109].
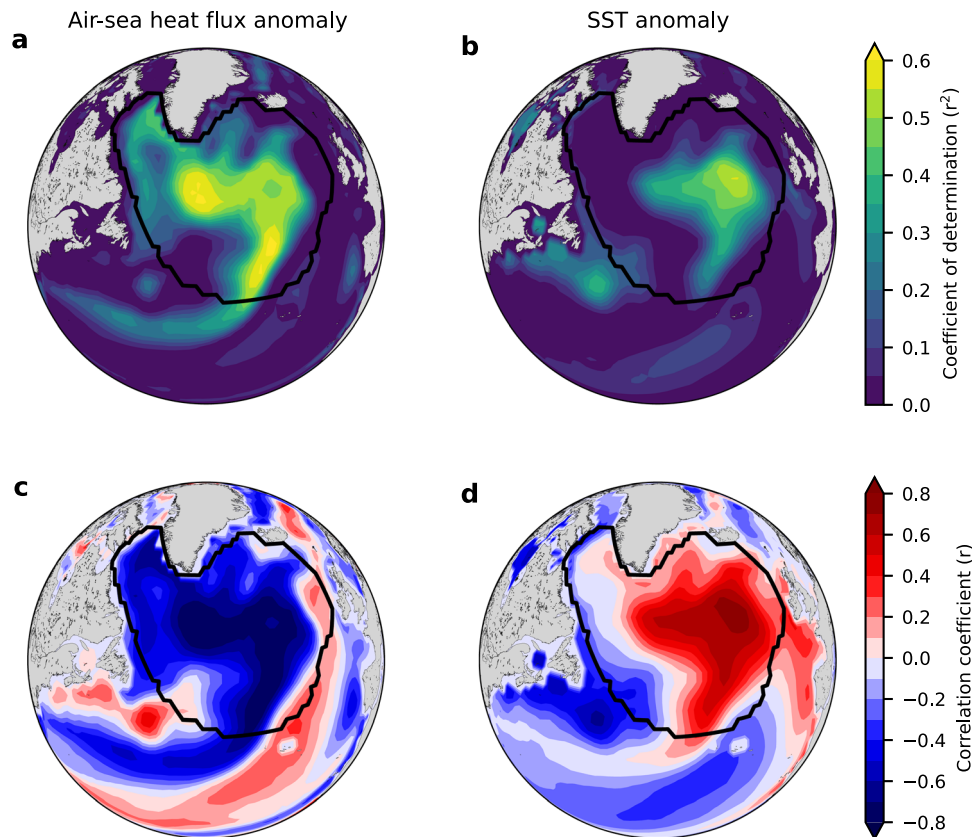
Fig. 7 | Correlation between decadal averaged AMOC anomalies at 26.5 °C and decadal averaged local SST and air-sea heat flux anomalies across climate models from CMIP6. Atlantic Meridional Overturning Circulation (AMOC) anomalies are calculated at 26.5°N for 24 climate models individually with respect to a linear trend over the time period in the pre-industrial AMOC simulations of each climate model that corresponds to the time period in the historical simulations. The North Atlantic air-sea flux anomalies are calculated for each model with respect to a linear trend of the North Atlantic air-sea heat fluxes over the time period in the pre-industrial simulations of each model that corresponds to the time period in the historical simulations. Sea surface temperature (SST) anomalies are calculated with respect to the globally averaged SST and averaged from November to May. Decadal averages of all anomalies were calculated over 15 decades from 1871 to 2020. Finally, the coefficient of determination between AMOC anomalies and **a** air-sea heat flux anomalies and **b** SST anomalies as well as the correlation coefficient between the AMOC anomalies and **c** air-sea heat flux anomalies and **d** SST anomalies are calculated. The black lines indicate the subpolar gyre region as defined by Caesar et al. [34]. The maps were produced using the Basemap tool in Python.

Discussion

While reconstructions based on air-sea heat flux anomalies have been shown here to be more robust than previous reconstructions based on SPG SST anomalies[34], they also come with limitations and caveats. The most important limitations are the limitations of the climate models in the CMIP6 ensemble, the limitations of the observation-based estimates, and consequently the limitations of the emergent constraint approach that exploits the link between air-sea heat flux and AMOC anomalies in climate models with the observation-based estimates of air-sea heat flux anomalies.

Limitations of climate models in simulating the ocean have been widely discussed, in particular for emergent constraints on ocean properties[22,47–50,110]. Climate models have, for example, horizontal and vertical resolution (Supplementary Fig. Table 1) that do not resolve mesoscale and sub-mesoscale processes[111–113], which affect the AMOC[37,114,115]. However, the relationship between air-sea heat flux anomalies and AMOC anomalies identified here exists over a wide range of model resolutions (Supplementary Table 1) from a coarse model resolution of 2° × 2.5° × 40 depth levels (GISS-E2.1-G) to an eddy-permitting resolution of 0.25° × 0.25° × 75 depth levels (GFDL-CM4), which gives confidence that our results are not specific to a coarse resolution model. In addition, climate models do not include all processes that are relevant for the AMOC and heat uptake in the North Atlantic. The most prominent process is likely the impact of freshwater input from the Greenland and Antarctic ice sheets, which are not dynamically included in climate models in CMIP6. Such ice sheet melting, when prescribed as a boundary flux in an ocean model with prescribed atmospheric forcing, can lead to an AMOC decrease at the OSNAP array of around 2 Sv until 2014[114]. A recent study, however, has demonstrated that the effect in a coupled Earth System Model is around 3 times smaller due to a compensating temperature feedback that cannot emerge in an ocean-only model[115]. Therefore, the missing ice sheet melts in the CMIP6 ensemble of coupled climate models likely plays a limited role.

Observational-based estimates have limitations as the available observations of atmospheric and sea surface temperatures lead to large uncertainties of the observation-based air-sea heat flux products. These uncertainties are most pronounced in the early part of each timeseries. As a result, the uncertainties of the reconstructed AMOC anomalies are relatively large (±2 Sv; 2-σ range). Within these uncertainties, the reconstructions of the AMOC based on ERA5 and JRA-55 are in agreement although decadal trends of the best estimates vary between both products (Fig. 9). However, a decline of the AMOC over the last 60 years appears to be unlikely given the increasing trend of the AMOC in both products since around 1990. Furthermore, additional air-sea heat flux from atmospheric warming would bias the reconstructed AMOC from ERA5 and JRA-55 towards too low anomalies since 1990 (Fig. 8 and Supplementary Fig. 6), which makes a decrease in the AMOC over the last three decades even more unlikely.
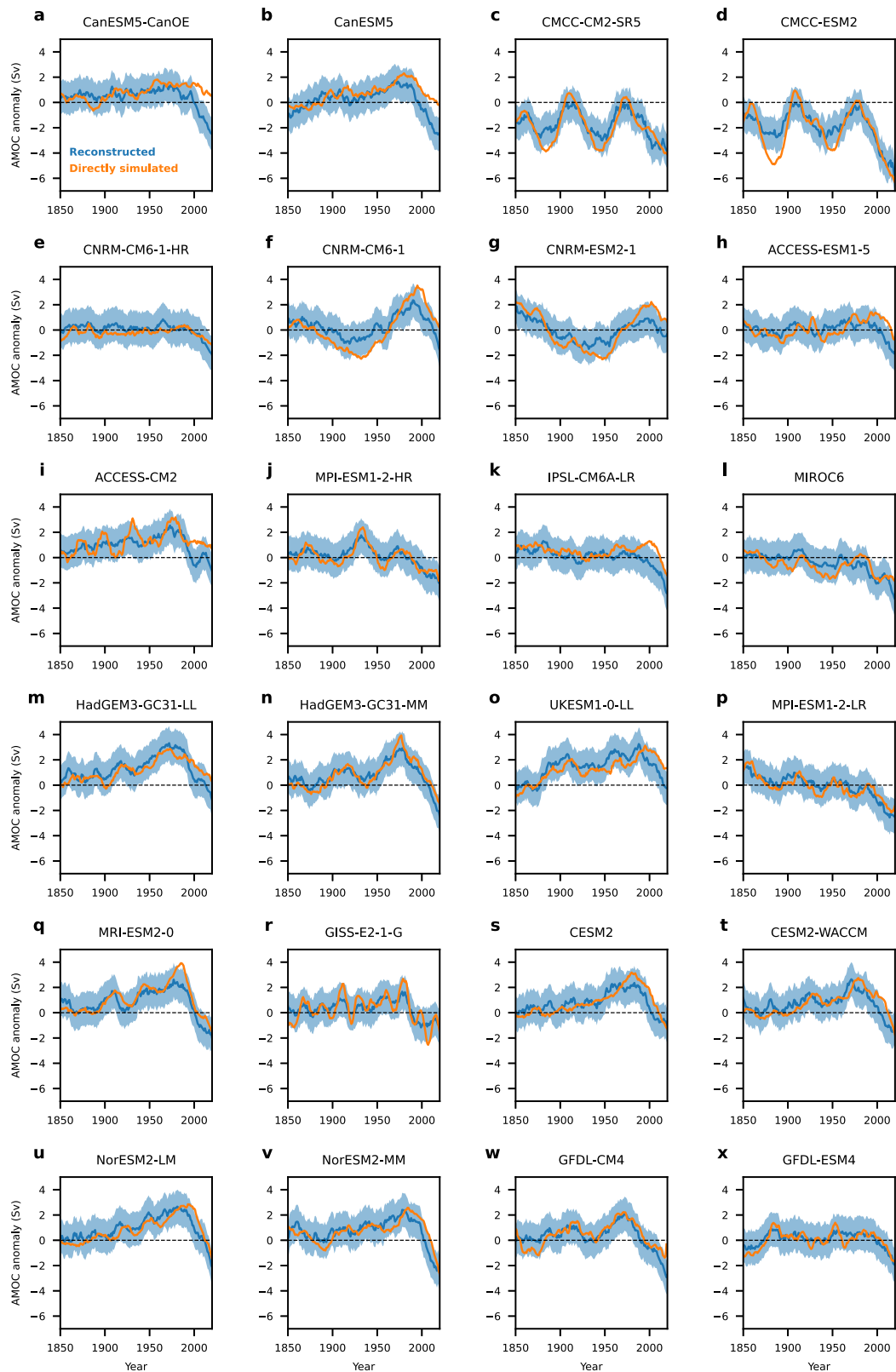
Fig. 8 | Directly simulated and reconstructed decadal averaged AMOC anomalies at 26.5°N in each model. The simulated decadal averaged Atlantic Meridional Overturning Circulation (AMOC) anomaly at 26.5°N (orange line) and the reconstructed AMOC anomalies at 26.5°N based on air-sea heat flux anomalies (blue line) for 24 climate models (**a–x**). The blue shading shows the 2-sigma standard deviation that results from the uncertainty of the linear fit. The dashed black line shows zero anomalies.
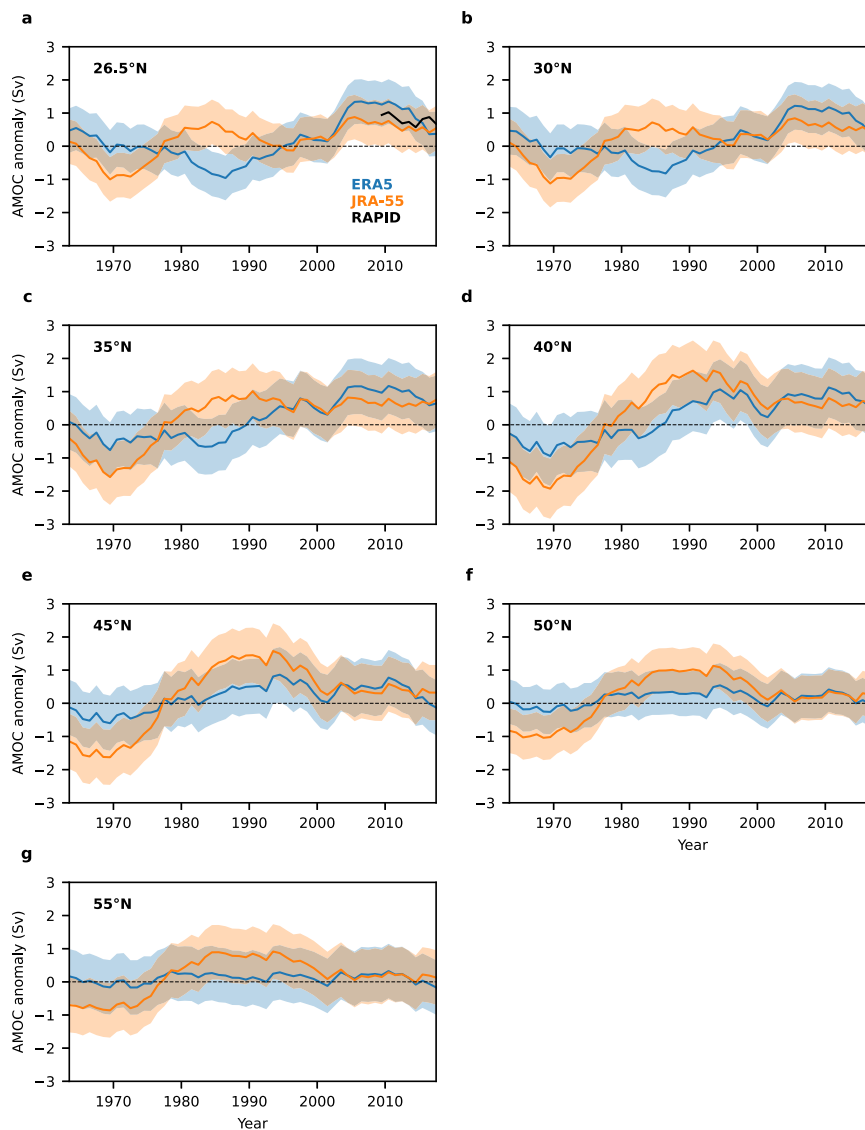
Fig. 9 | Constraining historical decadal AMOC variability across different latitudes. Reconstructed decadal averaged Atlantic Meridional Overturning Circulation (AMOC) anomalies with respect to the period from 1963 to 2017 at **a** 26.5°N, **b** 30°N, **c** 35°N, **d** 40°N, **e** 45°N, **f** 50°N, and **g** 55°N based on air-sea heat flux anomalies from ERA5 (blue) and JRA-55 (orange) integrated over the North Atlantic between that latitude and the Arctic Ocean (see "Methods" section for detailed description of the regions boundaries). Decadal averages from 2009 to 2017 are shown in (**a**) for the observed AMOC at the RAPID array (black). As the anomaly for the RAPID observations was calculated with respect to the mean over 2009 and 2017, we do not expect them to be at the same level on the y-axis as the anomaly of the reconstructed AMOC timeseries that were calculated with respect to the entire period from 1963 to 2017. For a better visual comparison of the time development and trend, we have hence added an offset of 0.8 Sv to the RAPID anomaly so that it is close to the two reconstructions in absolute magnitude. Shadings indicate the 1-σ uncertainty range based on uncertainties of the relationship between AMOC and air-sea heat flux anomalies across the model ensemble. Uncertainties from the observation-based estimates of the air-sea heat flux anomalies from the reanalysis products are not represented. Source data are provided as a Source Data file.

Table 1 | Coefficients of determination (r^2) and slope and intercept of the linear fit for AMOC anomalies and air-sea heat flux anomalies in the climate models

Latitude (°N)	Annual averages (1850–2016)			Decadal averages (1850s to 2010s)			1850–2016 averages		
	r^2	slope (10^{-21} Sv J^{-1})	intercept (Sv)	r^2	slope (10^{-21} Sv J^{-1})	intercept (Sv)	r^2	slope (10^{-21} Sv J^{-1})	intercept (Sv)
26.5	0.22	−0.30	0.28	0.74	−0.67	0.23	0.95	−0.70	0.23
30.0	0.20	−0.30	0.30	0.73	−0.70	0.25	0.93	−0.70	0.25
35.0	0.18	−0.33	0.30	0.72	−0.83	0.24	0.92	−0.83	0.25
40.0	0.15	−0.32	0.28	0.71	−0.96	0.25	0.90	−0.96	0.27
45.0	0.08	−0.25	0.18	0.70	−0.95	0.15	0.92	−0.91	0.18
50.0	0.04	−0.16	0.15	0.63	−0.76	0.13	0.86	−0.69	0.15
55.0	0.02	−0.15	0.10	0.39	−0.84	0.10	0.66	−0.82	0.12

Values are provided for annual averages, decadal, and long-term averages from 1850 to 2016 at a range of latitudes across the North Atlantic.

To reconstruct the AMOC based on a relationship across an ensemble of climate models, several conditions have to be met[56,57]: The relationship must be based on a plausible mechanism, and that mechanism must be verified, for example by additional output from the climate model ensemble, and the relationship must hold in out-of-sample testing. Here, we provide such a plausible mechanism (Figs. 4, 5 and 6) that is based on previous studies[32,34]. With the heat budget analysis in the North Atlantic, i.e., the northward heat flux anomalies and changes in the ocean heat content, we verify that this mechanism is indeed the underlying reason for the strong relationship between air-sea heat flux anomalies and AMOC anomalies on decadal and longer timescales. Finally, we tested our approach with out-of-sample testing for each model in the pre-industrial control simulations (Supplementary Figs. 7 and 8) and historical simulations (Fig. 8 and Supplementary Fig. 6) and also across CMIP5 climate models (Supplementary Fig. 9). These tests were successful for all climate models in the pre-industrial control simulations and for most climate models in the historical simulations. Due to anthropogenic warming in the last decades, a small bias of 1 Sv towards too low reconstructed AMOCs may arise once anthropogenic warming leads to additional air-sea heat flux anomalies that are not related to the AMOC. However, that bias is well within the uncertainties. Only the climate models with excessive ECS have reconstructed AMOC anomalies that are more than 2-sigma different from the directly simulated AMOC over the more recent decades. As only two models with unrealistic warming failed the test, the relationship or emergent constraint proposed here seems indeed to be robust but may lead to a small bias towards too negative AMOC anomalies from around 1990 to 2000.

The reconstructed decadal averaged AMOC appears to be less variable than the simulated AMOC in climate models and hence less sensitive to external forcing such as aerosols or greenhouse gases. Over the last 60 years, the reconstructed AMOC shows neither a sign of the simulated increase in the AMOC in 15 out of the 24 climate models in the second half of the 20th century nor of the simulated decline in the AMOC after 2000 that is simulated in 20 out of 24 climate models (Fig. 8). The initial increase of the AMOC in the climate models has been shown to be driven by increasing aerosol concentrations[90,116,117]. The increase in aerosols in models has been shown to alter wind patterns in a way that evaporation over the North Atlantic increases, which results in increased sea surface salinity and density, and consequently in stronger deep-water formation and Atlantic overturning[90,116,117], though this may also be a response to heat flux induced changes[91]. The later decline in the simulated AMOC across climate models, on the other hand, is caused by the warming of the North Atlantic ocean surface due to increasing greenhouse gases and a subsequent reduction in surface ocean density and deep-water formation[36]. The absence of such trends in the reconstructed AMOC indicates that the impact of aerosol and greenhouse gases are of a different strength than simulated in the climate models or that the AMOC is less sensitive to external forcing than previously thought[32,34]. The absence of the AMOC decrease in our reconstruction and the apparent robustness of the AMOC to external forcings is even more astonishing as meltwater fluxes from Greenland, which are not included in most climate models, are believed to also decrease the AMOC[32], albeit likely by a limited amount so far[115]. This apparent robustness of the AMOC over the recent decades raises the question if the projected AMOC decline across the CMIP6 model ensemble over the 21st century[36] may be too large due to an AMOC that is too sensitive in these climate models[118].

In addition to air-sea heat flux anomalies, other variables such as net surface buoyancy fluxes that incorporate both heat and freshwater fluxes could be used to improve the reconstructions of the AMOC. Multi-variable constraints[22] using heat and freshwater fluxes separately could also lead to further improvements. Here, we have not used freshwater fluxes due to large uncertainty in precipitation minus evaporation over the open ocean[99], and because the correlation between surface fluxes of heat and freshwater complicates the calibration of a multi-linear relationship using both of these flux products. Further research is needed to test if the addition of freshwater fluxes or salinity changes might further improve the reconstructed estimates of the AMOC anomaly.

Proxy-based reconstructions of AMOC variability at 26.5°N over the past century have yielded a range of possible timeseries, some that show a decline, and some that do not. Two recent review papers have attempted to detect any coherence in these records by combining AMOC variability across a range of proxies[44,119]. Unfortunately, these reviews disagree with one another: Moffa-Sanchez et al.[119] use a wide range of available proxies across the North Atlantic and find no coherent variability, while Caesar et al.[44] use a subset of the available proxies that the authors deem to be most robust and find a reduced AMOC strength starting in either the second half of the 19th century or the 1960s. The disagreement between these reviews revolves around which proxies should be considered[63,120] and whether using more proxies is appropriate. Our reconstructions cannot disentangle this issue but we do see limited evidence of a peak in the AMOC prior to the 1960s (Fig. 8) as proposed in Caesar et al.[44]. Similarly, we see no evidence of a long-term decline in the AMOC since the second half of the nineteenth century (Fig. 8) as proposed by Caesar et al.[44].

Overall, our study shows that the North Atlantic air-sea heat flux anomaly tracks AMOC variability on decadal and longer timescales, and is more robust than the previously-proposed SST-based AMOC proxy[34]. Over the next decades, air-sea heat flux anomaly observations will thus provide a complementary way to observe AMOC changes in addition to existing direct observations at mooring arrays. The air-sea heat flux derived AMOC estimates are best suited to reconstruct AMOC variability in the subtropical North Atlantic, but also closely track the northward meridional heat transport in the subtropical and subpolar North Atlantic up to 50°N. The varying AMOC reconstructions at different latitudes also show that the AMOC is not a simple conveyor belt but strongly heterogeneous across latitudes[101,108,109]. Moreover, the new reconstructions of the AMOC strength over the last 60 years suggest that the AMOC is more stable than previously thought and that an AMOC decline has not occurred yet.

Methods
Earth System Models
The 24 Earth System Models (Supplementary Table 1) in the main part of this study are all part of phase 6 of the Coupled Model Intercomparison Project (CMIP6). These 24 climate models were selected based on the availability of all necessary output variables (Meridional overturning stream function in latitude-depth coordinates, surface ocean temperature, air-sea heat fluxes, and interior ocean potential temperatures) in the pre-industrial control simulation, the historical simulation, and the SSP1-2.6 and SSP5-8.5 scenarios. One ensemble member is used per model. In addition, simulated northward heat transport in the North Atlantic was used to corroborate the proposed mechanism in the manuscript. This variable was only available for 18 of the 24 ESMs. To test our results in a different model ensemble, we downloaded data from all CMIP5 models for which we found all necessary variables (Supplementary Table 2). As the historical period in CMIP5 ended in 2005, we used output from Representative Concentration Pathway 8.5[121] simulations afterwards.

From each climate model, all output variables were downloaded and analysed on their native grid when available. Only 3-D output from NorESM2-LM and NorESM2-MM was downloaded in its regridded form because these two models use vertical density coordinates and not depth coordinates.

Output was downloaded for the historical simulations and projections under the low-emission, high-mitigation Shared Socioeconomic Pathway (SSP) 1-2.6 and the high-emission, low mitigation SSP5-8.5[122]. In addition, output from the respective pre-industrial control simulation was downloaded for the timesteps that correspond

to the years 1850 to 2100 in the historical and SSP simulations to quantify the drift in each variable. The drift was estimated by fitting a linear regression over the 250 years of this pre-industrial simulation for each variable. This linear fit over the pre-industrial control simulation was then subtracted from the respective historical and SSP simulations to calculate anomalies.

Processing of Earth System Model output

Monthly output from climate models was used to calculate annual averages of the maximum AMOC strength at various latitudes, the basin-wide integrated air-sea heat fluxes in the North Atlantic, the northward heat transport in the Atlantic basin across various latitudes, and the SPG SST index as defined by Caesar et al. [34] (black lines in Fig. 7).

The annually averaged AMOC at each latitude was calculated as the average of the monthly maxima of the streamfunction (CMIP6 variables 'msftmz' or 'msftyz' depending on the model) at that latitude below 500 m. The first 500 m were excluded to avoid a temporary wind-generated peak in northward water flow that might be wrongly identified as the AMOC maximum.

The northward heat flux at a given latitude in the North Atlantic is an output variable for each model ('hfbasin') so no further calculation was necessary.

The basin-wide annually averaged total air-sea heat fluxes ('hfds') were integrated over the North Atlantic. The North Atlantic was here defined as the region north of a given latitude (varying from 26.5°N to 55°N) and south of the Fram Strait, the Barents Sea Opening, and the Davis Straits. The Hudson Bay and the Mediterranean Sea are not included in the definition of the North Atlantic Ocean.

The annual SPG SST index was calculated following Caesar et al. [34] as the anomaly of the average SST in the subpolar gyre with respect to the globally averaged SST. These anomalies were then averaged in time over the months of November to May with the year of the SPG SST index corresponding to the year in November.

Anomalies of the AMOC, the northward heat transport, the air-sea heat flux, and the SPG and global SSTs were calculated as the difference between the historical plus projection simulations and the linear fit through the pre-industrial control simulation.

Reconstructing the AMOC based on observation-based air-sea heat fluxes

To reconstruct AMOC anomalies, a linear regression with prediction intervals between the AMOC anomalies and the air-sea heat flux anomalies was fitted across output from all 24 climate models. As almost all regressions are statistically significant ($p < 0.05$), we only highlight the non-significant relationships throughout the manuscript. Fits were made for annual output, decadal averaged output, and output averaged from 1850 to 2016. In addition, 1-σ projection intervals were calculated. We did not include years after 2016 as this is the year until which Caesar et al. estimated the AMOC decline based on the SPG SST index[34]. In addition, decadal averages were chosen in accordance and were calculated for the 17 decades in each model starting with the decade from 1850 to 1860 and ending with the decade from 2010 to 2020. As historical simulations in CMIP6 finish in 2014, the output for the years from 2015 to 2020 was taken from SSP5-8.5. The high-emission SSP was chosen because it is the only SSP for which all climate models provide output. In addition, differences in the radiative forcing in 2020 between SSP1-2.6 and SSP5-8.5 are only 0.15 W m^{-2} and differences in atmospheric CO_2 are 2.7 ppm[122]. These differences in the first years of the SSPs are too small to create substantial differences in the overall climate, and especially the AMOC, air-sea heat fluxes, and SSTs until 2020.

The linear relationship between the air-sea heat flux and AMOC anomalies was then exploited with observation-based estimates of air-sea heat flux anomalies to reconstruct AMOC anomalies based on

previous studies using the concept of emergent constraints[22,47–49,51]. To that extent, the probability distribution functions of the estimate of the air-sea heat flux and that of the linear fit were convoluted. Both probability distribution functions are assumed to be Gaussian. The resulting 2-D probability function is then projected on the y-axis (the AMOC anomaly) so that the best estimate and the uncertainties of the AMOC anomaly can be calculated.

As robust relationships could not be identified for annual anomalies (Fig. 3), only decadal and centennial AMOC anomalies were reconstructed here. Decadal averaged AMOC estimates were reconstructed based on the linear regression across decadal averages from climate models and based on decadal averages of monthly gridded North Atlantic air-sea heat fluxes from ERA5[65] and JRA-55[66]. ERA5 heat fluxes are available from 1940 to 2022 and JRA-55 heat fluxes are available from 1958 to 2022. Anomalies for both estimates were calculated by subtracting the average air-sea heat fluxes from 1963 to 2017 as decadal averages of the air-sea heat flux in these years are available for both estimates and hence allow a comparison. Decadal averaged fluxes in each year were here calculated by averaging over all air-sea-heat fluxes within ±5 years around the respective year. The five years in the beginning and the end of the timeseries were excluded because no entire decadal averages could be calculated at the beginning and the end of the timeseries.

Testing the AMOC reconstruction with climate models

The reconstruction of the AMOC based on air-sea heat fluxes was tested with climate models. These tests were performed with each climate model separately (Fig. 8 and Supplementary Fig. 6). In each test, the linear regression was performed across an ensemble of 23 climate models after removing one model. The linear regression was then exploited with the air-sea heat flux anomalies from the excluded model. The so reconstructed AMOC anomaly for that excluded model was then compared to the directly simulated AMOC anomaly in that model. In addition, the AMOC was reconstructed for 5 CMIP5 models (Supplementary Fig. 9). As these models were not used for the calibration of the relationship, the linear regression across an ensemble of all 24 climate models from CMIP6 was used.

We further tested the reconstructions using the pre-industrial control simulations of each model. For these simulations without increasing atmospheric greenhouse gases and without climate change, we also find a strong correlation ($r^2 = 0.67$) between both anomalies on decadal timescales and a weak to non-existent relationship ($r^2 = 0.06$) on annual timescales (Supplementary Fig. 11). Centennial anomalies are zero as no anomaly exists in the AMOC and/or air-sea heat fluxes when averaging over long-time periods in the absence of climate change. Based on the relationship between decadal anomalies, we also robustly reconstructed the AMOC anomalies in each model (Supplementary Fig. 7) with differences between the reconstructed and directly simulated AMOC being smaller than 2σ (Supplementary Fig. 8).

Data availability

All climate model output is freely available online on the website of the World Climate Research programme (https://esgf-node.llnl.gov/projects/cmip6/). The ERA5 air-sea heat flux estimates are made freely available by the Copernicus Climate Change Service from the European Union (https://cds.climate.copernicus.eu/cdsapp#!/dataset/reanalysis-era5-single-levels-monthly-means?tab=overview). The JRA-55 air-sea heat flux estimates are made freely available by the Data Integration and Analysis System in Japan (https://search.diasjp.net/en/dataset/JRA55). The observational data from the RAPID array is freely available here (https://rapid.ac.uk/data.php). The post-processed CMIP6 timeseries are all freely available under (https://doi.org/10.17882/103457). The reconstructed AMOC anomalies based on air-sea heat flux anomalies from ERA5 and JRA-55 at various latitudes (Fig. 9) are freely available in the attached Source Data file. Correspondence

and requests for materials should be addressed to J.T. (jen-s.terhaar@unibe.ch). Source data are provided with this paper.

Code availability

The code for producing the figures of this study is available upon request from the corresponding author.

References

1. McCarthy, G. D. et al. Measuring the atlantic meridional over-turning circulation at 26°N. *Prog. Oceanogr.* **130**, 91–111 (2015).
2. Yin, J., Griffies, S. M., Winton, M., Zhao, M. & Zanna, L. Response of storm-related extreme sea level along the U.S. Atlantic Coast to combined weather and climate forcing. *J. Clim.* **33**, 3745–3769 (2020).
3. Sigmond, M., Fyfe, J. C., Saenko, O. A. & Swart, N. C. Ongoing AMOC and related sea-level and temperature changes after achieving the Paris targets. *Nat. Clim. Chang.* **10**, 672–677 (2020).
4. Jackson, L. C. et al. Global and European climate impacts of a slowdown of the AMOC in a high resolution GCM. *Clim. Dyn.* **45**, 3299–3316 (2015).
5. Yin, J., Schlesinger, M. E. & Stouffer, R. J. Model projections of rapid sea-level rise on the northeast coast of the United States. *Nat. Geosci.* **2**, 262–266 (2009).
6. Levermann, A., Griesel, A., Hofmann, M., Montoya, M. & Rahmstorf, S. Dynamic sea level changes following changes in the thermohaline circulation. *Clim. Dyn.* **24**, 347–354 (2005).
7. Rahmstorf, S. & Ganopolski, A. Long-term global warming scenarios computed with an efficient coupled climate model. *Clim. Chang.* **43**, 353–367 (1999).
8. Vellinga, M. & Wood, R. A. Global climatic impacts of a collapse of the Atlantic thermohaline circulation. *Clim. Chang.* **54**, 251–267 (2002).
9. Manabe, S. & Stouffer, R. J. The role of thermohaline circulation in climate. *Tellus B Chem. Phys. Meteorol.* https://doi.org/10.3402/tellusb.v51i1.16262 (1999).
10. Stouffer, R. J. et al. Investigating the causes of the response of the thermohaline circulation to past and future climate changes. *J. Clim.* **19**, 1365–1387 (2006).
11. Schwinger, J., Asaadi, A., Goris, N. & Lee, H. Possibility for strong northern hemisphere high-latitude cooling under negative emissions. *Nat. Commun.* **13**, 1095 (2022).
12. Trenberth, K. E., Zhang, Y., Fasullo, J. T. & Cheng, L. Observation-based estimates of global and basin ocean meridional heat transport time series. *J. Clim.* **32**, 4567–4583 (2019).
13. Bellomo, K., Angeloni, M., Corti, S. & von Hardenberg, J. Future climate change shaped by inter-model differences in Atlantic Meridional Overturning Circulation response. *Nat. Commun.* **12**, 3659 (2021).
14. Zhang, R. et al. A review of the role of the Atlantic Meridional Overturning Circulation in Atlantic multidecadal variability and associated climate impacts. *Rev. Geophys.* **57**, 316–375 (2019).
15. Petit, T., Lozier, M. S., Josey, S. A. & Cunningham, S. A. Atlantic deep water formation occurs primarily in the Iceland Basin and Irminger Sea by local buoyancy forcing. *Geophys. Res. Lett.* **47**, e2020GL091028 (2020).
16. Lozier, M. S. Deconstructing the conveyor belt. *Science* **328**, 1507–1511 (2010).
17. Heuzé, C. North Atlantic deep water formation and AMOC in CMIP5 models. *Ocean Sci.* **13**, 609–622 (2017).
18. Joos, F., Plattner, G.-K., Stocker, T. F., Marchal, O. & Schmittner, A. Global warming and marine carbon cycle feedbacks on future atmospheric CO_2. *Science* **284**, 464–467 (1999).
19. Brown, P. J. et al. Circulation-driven variability of Atlantic anthropogenic carbon transports and uptake. *Nat. Geosci.* **14**, 571–577 (2021).
20. Huber, M. B. & Zanna, L. Drivers of uncertainty in simulated ocean circulation and heat uptake. *Geophys. Res. Lett.* **44**, 1402–1413 (2017).
21. Goris, N. et al. Constraining projection-based estimates of the future North Atlantic carbon uptake. *J. Clim.* **31**, 3959–3978 (2018).
22. Terhaar, J., Frölicher, T. L. & Joos, F. Observation-constrained estimates of the global ocean carbon sink from Earth System Models. *Biogeosciences* **19**, 4431–4457 (2022).
23. Pérez, F. F. et al. Atlantic Ocean CO2 uptake reduced by weakening of the meridional overturning circulation. *Nat. Geosci.* **6**, 146–152 (2013).
24. Alley, R. B. The Younger Dryas cold interval as viewed from central Greenland. *Quat. Sci. Rev.* **19**, 213–226 (2000).
25. Broecker, W. S., Peteet, D. M. & Rind, D. Does the ocean–atmosphere system have more than one stable mode of operation? *Nature* **315**, 21–26 (1985).
26. Frajka-Williams, E. et al. *Atlantic Meridional Overturning Circulation observed by the RAPID-MOCHA-WBTS (RAPID-Meridional Overturning Circulation and Heatflux Array-Western Boundary Time Series) array at 26N from 2004 to 2020 (v2020.1)* https://doi.org/10.5285/cc1e34b3-3385-662b-e053-6c86abc03444 (2021).
27. Srokosz, M. A. & Bryden, H. L. Observing the Atlantic Meridional Overturning Circulation yields a decade of inevitable surprises. *Science* **348**, 1255575 (2015).
28. Susan Lozier, M. et al. Overturning in the Subpolar North Atlantic Program: a new International Ocean Observing System. *Bull. Am. Meteorol. Soc.* **98**, 737–752 (2017).
29. Thornalley, D. J. R. et al. Anomalously weak Labrador Sea convection and Atlantic overturning during the past 150 years. *Nature* **556**, 227–230 (2018).
30. Spooner, P. T. et al. Exceptional 20th Century Ocean Circulation in the Northeast Atlantic. *Geophys. Res. Lett.* **47**, e2020GL087577 (2020).
31. Thibodeau, B. et al. Last century warming over the Canadian Atlantic shelves linked to weak Atlantic Meridional Overturning Circulation. *Geophys. Res. Lett.* **45**, 12,312–376,385 (2018).
32. Rahmstorf, S. et al. Exceptional twentieth-century slowdown in Atlantic Ocean overturning circulation. *Nat. Clim. Chang.* **5**, 475–480 (2015).
33. Sherwood, O. A., Lehmann, M. F., Schubert, C. J., Scott, D. B. & McCarthy, M. D. Nutrient regime shift in the western North Atlantic indicated by compound-specific δ15N of deep-sea gorgonian corals. *Proc. Natl Acad. Sci. USA* **108**, 1011–1015 (2011).
34. Caesar, L., Rahmstorf, S., Robinson, A., Feulner, G. & Saba, V. Observed fingerprint of a weakening Atlantic Ocean overturning circulation. *Nature* **556**, 191–196 (2018).
35. Worthington, E. L. et al. A 30-year reconstruction of the Atlantic Meridional Overturning Circulation shows no decline. *Ocean Sci.* **17**, 285–299 (2021).
36. Weijer, W., Cheng, W., Garuba, O. A., Hu, A. & Nadiga, B. T. CMIP6 models predict significant 21st century decline of the Atlantic Meridional Overturning Circulation. *Geophys. Res. Lett.* **47**, e2019GL086075 (2020).
37. Hirschi, J. J.-M. et al. The Atlantic Meridional Overturning Circulation in high-resolution models. *J. Geophys. Res. Ocean.* **125**, e2019JC015522 (2020).
38. Jackson, L. C. et al. Understanding AMOC stability: the North Atlantic Hosing Model Intercomparison Project. *Geosci. Model Dev.* **16**, 1975–1995 (2023).
39. Jackson, L. C. et al. The evolution of the North Atlantic Meridional Overturning Circulation since 1980. *Nat. Rev. Earth Environ.* **3**, 241–254 (2022).
40. Latif, M., Sun, J., Visbeck, M. & Hadi Bordbar, M. Natural variability has dominated Atlantic Meridional Overturning Circulation since 1900. *Nat. Clim. Chang.* **12**, 455–460 (2022).

41. Ridge, S. M. & McKinley, G. A. Advective controls on the North Atlantic anthropogenic carbon sink. *Glob. Biogeochem. Cycles* **34**, e2019GB006457 (2020).

42. Lobelle, D., Beaulieu, C., Livina, V., Sévellec, F. & Frajka-Williams, E. Detectability of an AMOC decline in current and projected climate changes. *Geophys. Res. Lett.* **47**, e2020GL089974 (2020).

43. Zhu, C., Liu, Z., Zhang, S. & Wu, L. Likely accelerated weakening of Atlantic overturning circulation emerges in optimal salinity fingerprint. *Nat. Commun.* **14**, 1245 (2023).

44. Caesar, L., McCarthy, G. D., Thornalley, D. J. R., Cahill, N. & Rahmstorf, S. Current Atlantic Meridional Overturning Circulation weakest in last millennium. *Nat. Geosci.* **14**, 118–120 (2021).

45. Cox, P. M., Huntingford, C. & Williamson, M. S. Emergent constraint on equilibrium climate sensitivity from global temperature variability. *Nature* **553**, 319–322 (2018).

46. Wenzel, S., Cox, P. M., Eyring, V. & Friedlingstein, P. Emergent constraints on climate-carbon cycle feedbacks in the CMIP5 Earth system models. *J. Geophys. Res. Biogeosci.* **119**, 794–807 (2014).

47. Terhaar, J., Kwiatkowski, L. & Bopp, L. Emergent constraint on Arctic Ocean acidification in the twenty-first century. *Nature* **582**, 379–383 (2020).

48. Terhaar, J., Frölicher, T. & Joos, F. Southern Ocean anthropogenic carbon sink constrained by sea surface salinity. *Sci. Adv.* **7**, 5964–5992 (2021).

49. Terhaar, J., Torres, O., Bourgeois, T. & Kwiatkowski, L. Arctic Ocean acidification over the 21st century co-driven by anthropogenic carbon increases and freshening in the CMIP6 model ensemble. *Biogeosciences* **18**, 2221–2240 (2021).

50. Kwiatkowski, L. et al. Emergent constraints on projections of declining primary production in the tropical oceans. *Nat. Clim. Chang.* **7**, 355–358 (2017).

51. Cox, P. M. et al. Sensitivity of tropical carbon to climate change constrained by carbon dioxide variability. *Nature* **494**, 341–344 (2013).

52. Schlund, M., Lauer, A., Gentine, P., Sherwood, S. C. & Eyring, V. Emergent constraints on equilibrium climate sensitivity in CMIP5: do they hold for CMIP6? *Earth Syst. Dyn.* **11**, 1233–1258 (2020).

53. Caldwell, P. M. et al. Statistical significance of climate sensitivity predictors obtained by data mining. *Geophys. Res. Lett.* **41**, 1803–1808 (2014).

54. Brient, F. Reducing uncertainties in climate projections with emergent constraints: concepts, examples and prospects. *Adv. Atmos. Sci.* **37**, 1–15 (2020).

55. Sanderson, B. M. et al. The potential for structural errors in emergent constraints. *Earth Syst. Dyn.* **12**, 899–918 (2021).

56. Hall, A., Cox, P., Huntingford, C. & Klein, S. Progressing emergent constraints on future climate change. *Nat. Clim. Chang.* **9**, 269–278 (2019).

57. Eyring, V. et al. Taking climate model evaluation to the next level. *Nat. Clim. Chang.* **9**, 102–110 (2019).

58. Fraser, N. J. & Cunningham, S. A. 120 years of AMOC variability reconstructed from observations using the Bernoulli inverse. *Geophys. Res. Lett.* **48**, e2021GL093893 (2021).

59. Rossby, T., Chafik, L. & Houpert, L. What can hydrography tell us about the strength of the Nordic Seas MOC over the last 70 to 100 years? *Geophys. Res. Lett.* **47**, e2020GL087456 (2020).

60. Rossby, T., Palter, J. & Donohue, K. What can hydrography between the New England slope, Bermuda and Africa tell us about the strength of the AMOC over the last 90 years? *Geophys. Res. Lett.* **49**, e2022GL099173 (2022).

61. Little, C. M., Zhao, M. & Buckley, M. W. Do surface temperature indices reflect centennial-timescale trends in Atlantic Meridional Overturning Circulation strength? *Geophys. Res. Lett.* **47**, e2020GL090888 (2020).

62. Li, L., Lozier, M. S. & Li, F. Century-long cooling trend in subpolar North Atlantic forced by atmosphere: an alternative explanation. *Clim. Dyn.* **58**, 2249–2267 (2022).

63. Kilbourne, K. H. et al. Atlantic circulation change still uncertain. *Nat. Geosci.* **15**, 165–167 (2022).

64. Keil, P. et al. Multiple drivers of the North Atlantic warming hole. *Nat. Clim. Chang.* **10**, 667–671 (2020).

65. Hersbach, H. et al. The ERA5 global reanalysis. *Q. J. R. Meteorol. Soc.* **146**, 1999–2049 (2020).

66. Kobayashi, S. et al. The JRA-55 reanalysis: general specifications and basic. *Charact. J. Meteorol. Soc. Jpn. Ser. II* **93**, 5–48 (2015).

67. Menary, M. B. et al. Aerosol-forced AMOC changes in CMIP6 historical simulations. *Geophys. Res. Lett.* **47**, e2020GL088166 (2020).

68. Ditlevsen, P. & Ditlevsen, S. Warning of a forthcoming collapse of the Atlantic meridional overturning circulation. *Nat. Commun.* **14**, 4254 (2023).

69. Boers, N. Observation-based early-warning signals for a collapse of the Atlantic Meridional Overturning Circulation. *Nat. Clim. Chang.* **11**, 680–688 (2021).

70. Gulev, S. K., Latif, M., Keenlyside, N., Park, W. & Koltermann, K. P. North Atlantic Ocean control on surface heat flux on multidecadal timescales. *Nature* **499**, 464–467 (2013).

71. Ganachaud, A. & Wunsch, C. Improved estimates of global ocean circulation, heat transport and mixing from hydrographic data. *Nature* **408**, 453–457 (2000).

72. Trenberth, K. E. & Fasullo, J. T. Atlantic meridional heat transports computed from balancing Earth's energy locally. *Geophys. Res. Lett.* **44**, 1919–1927 (2017).

73. Bellomo, K. & Mehling, O. Impacts and state-dependence of AMOC weakening in a warming climate. *Geophys. Res. Lett.* **51**, e2023GL107624 (2024).

74. Robson, J., Sutton, R., Menary, M. B. & Lai, M. W. K. Contrasting internally and externally generated Atlantic Multidecadal Variability and the role for AMOC in CMIP6 historical simulations. *Philos. Trans. R. Soc. A Math. Phys. Eng. Sci.* **381**, 20220194 (2023).

75. Lai, W. K. M., Robson, J. I., Wilcox, L. J. & Dunstone, N. Mechanisms of internal atlantic multidecadal variability in HadGEM3-GC3.1 at two different resolutions. *J. Clim.* **35**, 1365–1383 (2022).

76. Danabasoglu, G., Landrum, L., Yeager, S. G. & Gent, P. R. Robust and nonrobust aspects of Atlantic Meridional Overturning Circulation variability and mechanisms in the community Earth system model. *J. Clim.* **32**, 7349–7368 (2019).

77. Yeager, S. & Danabasoglu, G. The origins of late-twentieth-century variations in the large-scale North Atlantic Circulation. *J. Clim.* **27**, 3222–3247 (2014).

78. Bryden, H. L. et al. Reduction in ocean heat transport at 26°N since 2008 cools the eastern subpolar gyre of the North Atlantic Ocean. *J. Clim.* **33**, 1677–1689 (2020).

79. Ganachaud, A. & Wunsch, C. Large-scale ocean heat and freshwater transports during the world ocean circulation experiment. *J. Clim.* **16**, 696–705 (2003).

80. Trenberth, K. E. & Caron, J. M. Estimates of meridional atmosphere and ocean heat transports. *J. Clim.* **14**, 3433–3443 (2001).

81. Johns, W. E. et al. Continuous, array-based estimates of Atlantic Ocean heat transport at 26.5°N. *J. Clim.* **24**, 2429–2449 (2011).

82. Piecuch, C. G., Ponte, R. M., Little, C. M., Buckley, M. W. & Fukumori, I. Mechanisms underlying recent decadal changes in subpolar North Atlantic Ocean heat content. *J. Geophys. Res. Ocean.* **122**, 7181–7197 (2017).

83. Foukal, N. P. & Lozier, M. S. Assessing variability in the size and strength of the North Atlantic subpolar gyre. *J. Geophys. Res. Ocean.* **122**, 6295–6308 (2017).

84. WALIN, G. On the relation between sea-surface heat flow and thermal circulation in the ocean. *Tellus* **34**, 187–195 (1982).

85. Speer, K. & Tziperman, E. Rates of water mass formation in the North Atlantic Ocean. *J. Phys. Oceanogr.* **22**, 93–104 (1992).

86. Desbruyères, D. G., Mercier, H., Maze, G. & Daniault, N. Surface predictor of overturning circulation and heat content change in the subpolar North Atlantic. *Ocean Sci.* **15**, 809–817 (2019).

87. Kostov, Y., Johnson, H. L. & Marshall, D. P. AMOC sensitivity to surface buoyancy fluxes: the role of air-sea feedback mechanisms. *Clim. Dyn.* **53**, 4521–4537 (2019).

88. Megann, A., Blaker, A., Josey, S., New, A. & Sinha, B. Mechanisms for late 20th and early 21st century decadal AMOC variability. *J. Geophys. Res. Ocean.* **126**, e2021JC017865 (2021).

89. Grist, J. P., Marsh, R. & Josey, S. A. On the relationship between the North Atlantic Meridional Overturning Circulation and the surface-forced overturning streamfunction. *J. Clim.* **22**, 4989–5002 (2009).

90. Hassan, T., Allen, R. J., Liu, W. & Randles, C. A. Anthropogenic aerosol forcing of the Atlantic meridional overturning circulation and the associated mechanisms in CMIP6 models. *Atmos. Chem. Phys.* **21**, 5821–5846 (2021).

91. Robson, J. et al. The role of Anthropogenic Aerosol Forcing in the 1850–1985 strengthening of the AMOC in CMIP6 historical simulations. *J. Clim.* **35**, 6843–6863 (2022).

92. Chiang, J. C. H., Cheng, W., Kim, W. M. & Kim, S. Untangling the relationship between AMOC variability and North Atlantic upper-ocean temperature and salinity. *Geophys. Res. Lett.* **48**, e2021GL093496 (2021).

93. Buckley, M. W. & Marshall, J. Observations, inferences, and mechanisms of the Atlantic Meridional Overturning Circulation: a review. *Rev. Geophys.* **54**, 5–63 (2016).

94. Drews, A. & Greatbatch, R. J. Evolution of the Atlantic multidecadal variability in a model with an improved North Atlantic current. *J. Clim.* **30**, 5491–5512 (2017).

95. Cheng, L. et al. Past and future ocean warming. *Nat. Rev. Earth Environ.* **3**, 776–794 (2022).

96. Tokarska Katarzyna, B. et al. Past warming trend constrains future warming in CMIP6 models. *Sci. Adv.* **6**, eaaz9549 (2021).

97. Sherwood, S. C. et al. An assessment of Earth's climate sensitivity using multiple lines of evidence. *Rev. Geophys.* **58**, e2019RG000678 (2020).

98. Nijsse, F. J. M. M., Cox, P. M. & Williamson, M. S. Emergent constraints on transient climate response (TCR) and equilibrium climate sensitivity (ECS) from historical warming in CMIP5 and CMIP6 models. *Earth Syst. Dyn.* **11**, 737–750 (2020).

99. Yu, L. Global air–sea fluxes of heat, fresh water, and momentum: energy budget closure and unanswered questions. *Ann. Rev. Mar. Sci.* **11**, 227–248 (2019).

100. Williams, R. G., Roussenov, V., Smith, D. & Lozier, M. S. Decadal evolution of ocean thermal anomalies in the North Atlantic: the effects of Ekman, overturning, and horizontal transport. *J. Clim.* **27**, 698–719 (2014).

101. Zhang, R. Latitudinal dependence of Atlantic Meridional Overturning Circulation (AMOC) variations. *Geophys. Res. Lett.* **37**, L16703 (2010).

102. Kwon, Y.-O. & Frankignoul, C. Mechanisms of multidecadal Atlantic Meridional Overturning Circulation variability diagnosed in depth versus density space. *J. Clim.* **27**, 9359–9376 (2014).

103. Lozier, M. S. et al. A sea change in our view of overturning in the subpolar North Atlantic. *Science* **363**, 516–521 (2019).

104. Mecking, J. V. & Drijfhout, S. S. The decrease in ocean heat transport in response to global warming. *Nat. Clim. Chang.* **13**, 1229–1236 (2023).

105. Jackson, L. C. & Petit, T. North Atlantic overturning and water mass transformation in CMIP6 models. *Clim. Dyn.* **60**, 2871–2891 (2023).

106. Tsujino, H. et al. Evaluation of global ocean–sea-ice model simulations based on the experimental protocols of the Ocean Model Intercomparison Project phase 2 (OMIP-2). *Geosci. Model Dev.* **13**, 3643–3708 (2020).

107. Jackson, L. C. & Wood, R. A. Fingerprints for Early detection of changes in the AMOC. *J. Clim.* **33**, 7027–7044 (2020).

108. Bower, A. et al. Lagrangian views of the pathways of the Atlantic Meridional Overturning Circulation. *J. Geophys. Res. Ocean.* **124**, 5313–5335 (2019).

109. Bingham, R. J., Hughes, C. W., Roussenov, V. & Williams, R. G. Meridional coherence of the North Atlantic meridional overturning circulation. *Geophys. Res. Lett.* **34**, L23606 (2007).

110. Bourgeois, T., Goris, N., Schwinger, J. & Tjiputra, J. F. Stratification constrains future heat and carbon uptake in the Southern Ocean between 30°S and 55°S. *Nat. Commun.* **13**, 340 (2022).

111. Lachkar, Z., Orr, J. C. & Dutay, J.-C. Seasonal and mesoscale variability of oceanic transport of anthropogenic CO_2. *Biogeosciences* **6**, 2509–2523 (2009).

112. Lachkar, Z., Orr, J. C., Dutay, J.-C. & Delecluse, P. Effects of mesoscale eddies on global ocean distributions of CFC–11, CO_2, and $\Delta^{14}C$. *Ocean Sci.* **3**, 461–482 (2007).

113. Griffies, S. M. et al. Impacts on ocean heat from transient mesoscale eddies in a hierarchy of climate models. *J. Clim.* **28**, 952–977 (2015).

114. Swingedouw, D. et al. AMOC recent and future trends: a crucial role for oceanic resolution and Greenland melting? *Front. Clim.* **4**, 838310 (2022).

115. Martin, T. & Biastoch, A. On the ocean's response to enhanced Greenland runoff in model experiments: relevance of mesoscale dynamics and atmospheric coupling. *Ocean Sci.* **19**, 141–167 (2023).

116. Delworth, T. L. & Dixon, K. W. Have anthropogenic aerosols delayed a greenhouse gas-induced weakening of the North Atlantic thermohaline circulation? *Geophys. Res. Lett.* **33**, L02606 (2006).

117. Menary, M. B. et al. Mechanisms of aerosol-forced AMOC variability in a state of the art climate model. *J. Geophys. Res. Ocean.* **118**, 2087–2096 (2013).

118. McCarthy, G. D. & Caesar, L. Can we trust projections of AMOC weakening based on climate models that cannot reproduce the past? *Philos. Trans. R. Soc. A Math. Phys. Eng. Sci.* **381**, 20220193 (2023).

119. Moffa-Sánchez, P. et al. Variability in the Northern North Atlantic and Arctic Oceans across the last two millennia: a Review. *Paleoceanogr. Paleoclimatol.* **34**, 1399–1436 (2019).

120. Caesar, L., McCarthy, G. D., Thornalley, D. J. R., Cahill, N. & Rahmstorf, S. Reply to: Atlantic circulation change still uncertain. *Nat. Geosci.* **15**, 168–170 (2022).

121. van Vuuren, D. P. et al. The representative concentration pathways: an overview. *Clim. Change* **109**, 5 (2011).

122. Riahi, K. et al. The Shared Socioeconomic Pathways and their energy, land use, and greenhouse gas emissions implications: An overview. *Glob. Environ. Chang.* **42**, 153–168 (2017).

Acknowledgements

Author contributions

The idea for this study was conceived by J.T. A detailed outline was developed by J.T. and N.P.F. J.T. and L.V. performed the model output analysis, N.P.F. the analysis of the reanalysis data, and J.T. produced the figures. The initial manuscript was written by J.T. All authors contributed ideas, discussed the results, and wrote the manuscript.

Competing interests

The authors declare no competing interests.

Additional information

Supplementary information The online version contains supplementary material available at
https://doi.org/10.1038/s41467-024-55297-5.

Correspondence and requests for materials should be addressed to Jens Terhaar.

Peer review information *Nature Communications* thanks the anonymous reviewer(s) for their contribution to the peer review of this work. A peer review file is available.

Reprints and permissions information is available at
http://www.nature.com/reprints

Publisher's note Springer Nature remains neutral with regard to jurisdictional claims in published maps and institutional affiliations.